Journal of Solid State Chemistry 183 (2010) 1372–1379

Contents lists available at ScienceDirect

Journal of Solid State Chemistry

journal homepage: www.elsevier.com/locate/jssc

Stabilization of over-stoichiometric Mn^{4+} in layered $Na_{2/3}MnO_2$

R. Stoyanova [a,b,*], D. Carlier [b], M. Sendova-Vassileva [c], M. Yoncheva [a], E. Zhecheva [a], D. Nihtianova [a,d], C. Delmas [b]

[a] Institute of General and Inorganic Chemistry, Bulgarian Academy of Sciences, 1113 Sofia, Bulgaria
[b] ICMCB-CNRS, Université de Bordeaux, IPB-ENSCBP, 87 av. du Dr. A. Schweitzer, 33608 Pessac cedex, France
[c] Central Laboratory of Solar Energy and New Energy Sources, Bulgarian Academy of Sciences, Sofia, Bulgaria
[d] Central Laboratory of Mineralogy and Crystallography, Bulgarian Academy of Sciences, Acad. G. Bonchev Str. bl. 107, 1113 Sofia, Bulgaria

ARTICLE INFO

Article history:
Received 22 January 2010
Received in revised form
10 April 2010
Accepted 14 April 2010
Available online 18 April 2010

Keywords:
Layered oxides
Sodium manganates
Electron paramagnetic resonance spectroscopy
Raman spectroscopy

ABSTRACT

Sodium manganates with nominal composition $Na_{2/3}MnO_2$ were prepared by solid state reaction between Na_2CO_3 and $MnCO_3$ at 1000 °C. The composition and structure of Na_xMnO_2 were controlled by the rate of cooling from the temperature of preparation. This is a consequence of the capability of $Na_{2/3}MnO_2$ to accommodate over-stoichiometric Mn^{4+} ions up to 12.5%. Structural characterization was carried out by XRD powder diffractions, TEM analysis and Raman spectroscopy. The composition and oxidation state of manganese were determined by chemical analysis and magnetic susceptibility measurements. The manganese distribution in the layers was analysed using electron paramagnetic resonance (EPR) spectroscopy. By quenching from 1000 °C, the orthorhombic distorted modification is stabilized. A phase separation into orthorhombic and hexagonal modifications takes place when $Na_{2/3}MnO_2$ is slow cooled. The structure changes are concomitant with an increase in the oxidation state of Mn. The over-stoichiometric Mn^{4+} ions are accommodated in the hexagonal modification by creation of vacancies in the MnO_2-layers.

1. Introduction

Sodium manganese oxides with layered structure, Na_xMnO_2, have continuously attracted both research and industrial interests ever since 1970 [1–8]. This is a consequence of the diversity of their physical and chemical properties. From a physical point of view, Na_xMnO_2 oxides are considered as a model system for examination of magnetic and electrical properties in a two-dimensional hexagonal lattice [5–8]. The ability of Na_xMnO_2 to intercalate sodium as well as to exchange Na^+ for Li^+ determines their potential for practical applications in lithium (or sodium) rechargeable batteries [1–4,9]. The recent interest is based on the thermoelectric properties exhibited by layered sodium cobaltates, as well as on the discovery of the superconductivity of hydrated sodium cobaltates [5–7].

The studies on the crystal structure and composition of sodium manganese oxides began about 30 years ago [1,2,10]. In general, the structure of Na_xMnO_2 with $0.5 < x \leq 1$ consists of MnO_2-layers composed by edge-sharing MnO_6-octahedra [1,2,10]. Three types of stacking of oxygen were established for layered Na_xMnO_2: ABAABC (three MnO_2-layers in the unit cell), ABBA (two MnO_2-layers) and ABBCCA (three MnO_2-layers). The sodium ions are sandwiched between the MnO_2-layers so as to occupy octahedral or trigonal prismatic sites (denoted by *O* and *P*, respectively). Based on the number of the MnO_2-layers in the unit cell and the site occupied by Na, the structure of Na_xMnO_2 can be classified into three structural types: *P*2, *P*3 and *O*3 [10]. There is a close structural relation between *P*3 and *O*3: by gliding of the MnO_2-layer, the P3 structure is easily transformed to O3. On the contrary, the transformation of *P*2 to *P*3 requires breaking of Mn–O bonds.

The research group from Bordeaux was the first to report about sodium reacting with MnO_2 and forming compounds with a composition Na_xMnO_2 and a structure that depends on the Na content and the preparation temperature [1,2,9,10]. When the Na-to-Mn ratio is equal to 1, the *O*3 type structure is stabilized. Due to the appearance of Jahn–Teller Mn^{3+} ions, the layered structure is monoclinically distorted. With the decrease of the Na-to-Mn ratio from 1.0 to 0.7, the *P*2 structure becomes stable [1,2,11,12]. The charge compensation of the Na deficiency is achieved by Mn^{4+} ions: $Na_xMn_x^{3+}Mn_{1-x}^{4+}O_2$. However, the Mn^{3+} content is still high, leading to an orthorhombic distortion of *P*2. In addition, a monoclinic distortion of *P*2 has also been reported [12]. The extent of monoclinic distortion is small ($\beta = 90.68°$), which makes difficulties in distinguishing the orthorhombic and monoclinic distorted phases by means of XRD experiments [11,12]. At temperatures lower than 600 °C, $Na_{0.7}MnO_2$ is able to

* Corresponding author at: Institute of General and Inorganic Chemistry, Bulgarian Academy of Sciences, 1113 Sofia, Bulgaria. Fax: +359 2 870 50 24.
E-mail address: radstoy@svr.igic.bas.bg (R. Stoyanova).

0022-4596/$ - see front matter © 2010 Elsevier Inc. All rights reserved.
doi:10.1016/j.jssc.2010.04.024

uptake oxygen, as a result of which an undistorted *P*2 modification is isolated [1,2,11,12]. The *P*2 modification with a $Na_{0.7}MnO_{2+y}$ composition is stable for $0.05 < y < 0.25$, while the composition range of stability of the orthorhombic phase is $y < 0.05$. Keeping the Na-to-Mn ratio constant, the transformation from the orthorhombic modification to the hexagonal one is considered to be driven by the changes in the oxidation state of Mn ions, i.e. by depletion of the Mn^{3+} ions at the expense of Mn^{4+}. The Mn^{4+} ions which are needed to compensate the excess of oxygen are denoted as over-stoichiometric ions. Since a layered structure is derived from a close packing of oxygen atoms, Fouassier et al. [2] have proposed to formulate oxides as manganese deficient phases rather than oxygen excess phases: $Na_{0.70/(1+y)}Mn_{1/(1+y)}O_2$. The appearance of cation vacancies in $Na_{0.7}MnO_{2+y}$ has also been suggested by Bordet-Le Guenne et al. and Jeong et al. [11,13]. The formation of undistorted *P*2 modification is also sensitive towards the method of synthesis [14]: a sol–gel method allows preparing *P*2-modification of $Na_{0.6}MnO_2$ that is stable at temperature above 800 °C.

A temperature-induced variation of the oxygen stoichiometry has also been reported for layered sodium cobaltates and lithium manganate analogues [15,16]. Slow cooling of Na_xCoO_2 ($x \approx 0.65$) from 800 °C leads to the transformation of the orthorhombic phase to a hexagonal phase. This process is driven by Na exsolution from the Na-layers, as a result of which a separate Na_2CO_3 phase is formed [15]. On heating to 1000 °C, the reversible oxygen loss is limited to 1 wt% for $LiMnO_2$, while a higher reversible oxygen loss (up to 5 wt%) takes place for $Li_{2/3}Mn_{2/3}Ni_{1/3}O_2$ [16]. However, the peculiarities of the layered structure after oxygen loss are still unclear.

The question how the over-stoichiometric Mn^{4+} ions are stabilized in sodium manganates may be answered by using EPR spectroscopy (EPR). In $Na_{0.7}MnO_2$, there are two paramagnetic ions: Mn^{4+} and Mn^{3+} with half-integer and integer spin states, respectively ($S=3/2$ and $S=2$). It is well known that EPR spectroscopy in the X-band (9.3 GHz) is best suited for studying the electronic structure of ions with half-integer spin ground states, while ions with integer spin ground states are usually not active due to the higher magnitude of the zero field splitting parameter, *D*, as well as the shorter spin relaxation time [17]. However, this technique has been applied for studying the defect structure of lithium manganese spinels $Li_{1+x}Mn_{2-x}O_4$, containing both Mn^{4+} and Mn^{3+} ions, in respect of the method of synthesis (heating temperature, cooling rate, etc.) [18–23].

The aim of this contribution is to examine the stabilization of over-stoichiometric Mn^{4+} ions in $Na_{2/3}MnO_2$. The composition and structure of $Na_{2/3}MnO_2$ were changed by quenching of samples from 1000, 700 and 420 °C. The structural characterization was carried out by XRD powder diffractions, TEM analysis and Raman spectroscopy. The composition and oxidation state of manganese were determined by chemical analysis and magnetic susceptibility measurements. The manganese distribution in the layers was analysed using EPR spectroscopy. In order to understand the origin of the EPR spectra of $Na_{2/3}MnO_2$, we have used $Na_{2/3}Co_{2/3}Mn_{1/3}O_2$ as an EPR standard for Mn^{4+} ions surrounded by diamagnetic Co^{3+} and identical paramagnetic Mn^{4+} ions. This oxide is also isostructural to the hexagonal modification of $Na_{2/3}MnO_2$.

2. Experimental

Sodium manganates, $Na_{2/3}MnO_2$, were obtained at high temperatures by a solid state reaction between Na_2CO_3 and $MnCO_3$. The initial Na-to-Mn ratio was 0.70. The mixture of Na_2CO_3 and $MnCO_3$ was heated at 1000 °C for 15 h, followed by quenching to room temperature (*NMO-1000*). In addition, the sample heated at 1000 °C was cooled by 5°/min to 700 or to 420 °C, annealed at these temperatures for further 15 h and then quenched to room temperature (*NMO-700* and *NMO-420*). Oxides with $Na_{2/3}Co_{2/3}Mn_{1/3}O_2$ compositions were prepared by a co-precipitation method as described elsewhere [24].

The oxidation state of manganese was determined by iodometric titration against a standardized sodium thiosulfate solution. Iodometric titration was performed on 10–20 mg of sample in Ar atmosphere. For each composition titrations were repeated several times in order to obtain accurate and consistent results. This method has been used for the measurements of the average oxidation state of cobalt, nickel and manganese oxides with layered and perovskite structures [25,26]. The total content of manganese was established by complexometric analysis using eriochrome black *T* at pH=10.

X-ray structural analysis was made by a Bruker Advance D8 diffractometer with with detector Sol-X and using Cu*K*α radiation. Step-scan recordings for structure refinement by the Rietveld method were carried out using 0.03° 2θ steps of 10 s duration. The computer FullProf Suite Program (1.00) was used in the calculations [27].

The TEM investigations were performed by TEM JEOL 2100 with an accelerating voltage of 200 kV. The specimens were prepared by grinding and dispersing them in ethanol by ultrasonic treatment for 6 min. The suspensions were dripped on standard holey carbon/Cu grids.

The Raman spectra were recorded with a Horiba Jobin Yvon LabRAM HR800 spectrometer using the 600 l/mm grating and HeNe laser for excitation. The samples were placed under the 100× achromatic objective of a B×41 microscope and measured in back scattering configuration. The laser power on the sample was kept below 0.1 mW so that no heating effects on the powder sample could be observed. The IR spectra were recorded on a Fourier transform Nicolet Avatar-320 instrument using KBr pellets (resolution $< 2\,cm^{-1}$).

Magnetic susceptibility data of Na_xMnO_2 samples were collected on a Quantum Design MPMS-5S magnetometer in the range 5–340 K with a magnetic field of 5000 G.

The EPR spectra in the X-band (9.46 GHz) were recorded as a first derivative of the absorption signal of a Bruker spectrometer. The recording temperatures were varied between 5 and 300 K using a variable temperature insert (Oxford Instruments).

3. Results and discussions

3.1. Structural characterization of $Na_{2/3}MnO_2$

Fig. 1 shows the XRD patterns of *NMO-1000*, *NMO-700* and *NMO-700*. A single phase with the nominal composition $Na_{2/3}MnO_2$ is obtained by a solid state reaction at 1000 °C. The crystal structure of *NMO-1000* is refined in the orthorhombic *Cmcm* space group (Fig. 1), in accordance with XRD data of Bordet-Le Guenne et al. [11]. The refinement Na occupancy matches the total Na content used during the synthesis (Table 1). There are two positions for Na: the first Na position shares faces with MnO_6 octahedra in the layers above and below, while the second Na position shares edges only (Fig. 2). The six oxygen ions form the nearest environment of each Na ion, the *Na*(1) environment being more distorted: four *Na*(1)–O distances at 2.548 Å and two *Na*(1)–O distances at 2.334 Å as compared to 4 *Na*(2)–O distances at 2.428 Å and 2 *Na*(2)–O distances at 2.537 Å. The appearance of Mn ions just above and below the *Na*(1) sites leads to a shorter *Na*(1)–*Mn* distance of 2.805 Å, while Na(2) is surrounded by four Mn ions at a distance of 3.239 Å and two Mn

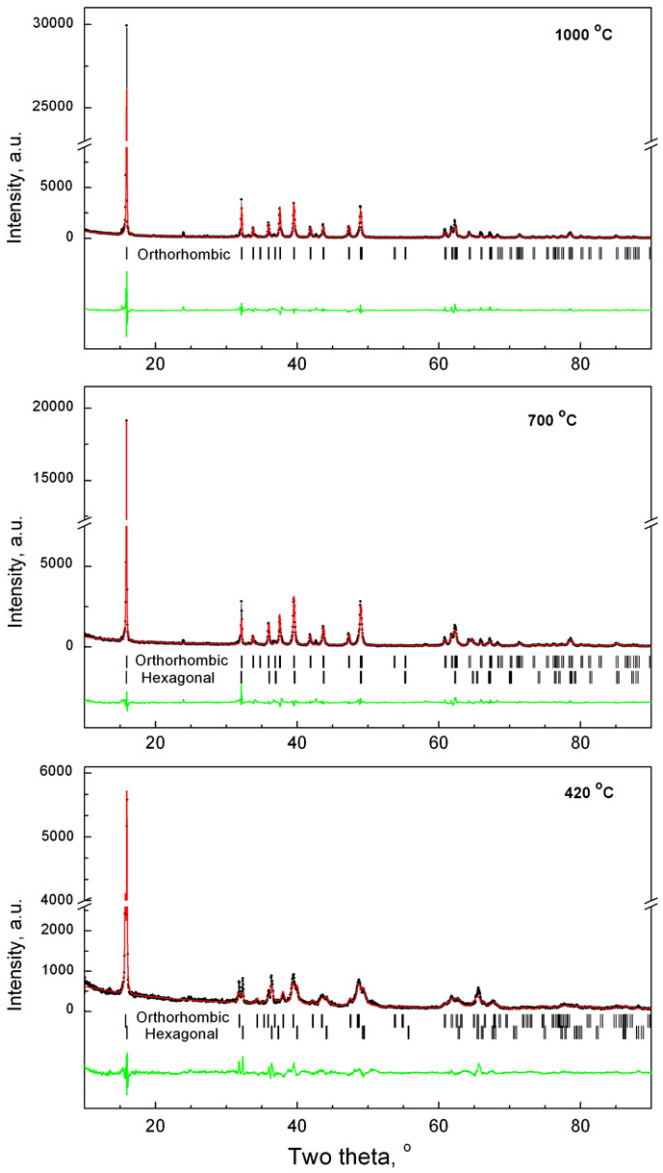

Fig. 1. XRD patterns of *NMO-1000*, *NMO-700* and *NMO-420*. The difference between the observed and calculated profiles is plotted. Bragg reflections for orthorhombic and hexagonal modifications are indicated.

ions at a distance of 3.279 Å. It is noticeable that the *Na*(1)–*Mn* distance is smaller in comparison with the distance between the identical ions (Mn–Mn or Na(1)–Na(1) and Na(2)–Na(2)) in the layers: 2.832 Å. The small *Na*(1)–*Mn* distance causes a significant Na–Mn repulsion, as a result of which the *Na*(1) site becomes energetically unfavourable as compared to the *Na*(2) site. In addition, the distance between the *Na*(1) and *Na*(2) sites in $Na_{2/3}MnO_2$is about 1.6 Å apart, which is about two times smaller than the ionic radius of Na. Therefore, it is energetically unfavourable when the nearest *Na*(1) and *Na*(2) sites are simultaneously occupied. This is consistent with different Na occupancies of two positions determined by structural analysis of $Na_{2/3}MnO_2$ (Table 1): *Na*(1) has 1/5 occupancy, while *Na*(2) has 1/2 occupancy. The sodium distribution over the two positions in $Na_{2/3}MnO_2$ bears resemblance with the Li and Na occupancy observed in structurally related $Na_{2/3}CoO_2$ and O2–$LiCoO_2$ [28,29]. The distribution of the alkaline ions can be described as a result from the competition between $Na^+(Li^+)$–$Co^{3+/4+}$ electrostatic

Table 1
Mean oxidation state of Mn (*OS*), phase amount of the orthorhombic modification (I_{ortho}, %), unit cell parameters (*a*, *b*, *c*) and Na and Mn site occupancy (*Na*(1), *Na*(2) and *Mn*) of $Na_{2/3}MnO_2$ quenched from 1000, 700 and 420 °C.

Samples	OS	I_{ortho}	*Cmcm*						*P6₃/mmc*				
	±	±2, %	*a* ± 0.0003, Å	*b* ± 0.0004, Å	*c* ± 0.0012, Å	*Na*(1) ± 0.02	*Na*(2) ± 0.02	Mn ± 0.01	*a* ± 0.0004, Å	*c* ± 0.0015, Å	*Na*(1) ± 0.03	Na(2) ± 0.03	Mn ± 0.02
NMO-1000	3.29	100	2.8317	5.3055	11.1387	0.21	0.49	1.00					
NMO-700	3.33	79	2.8321	5.3070	11.1367	0.18	0.50	1.00	2.8791	11.1632	0.40	0.29	0.91
NMO-420	3.65	58	2.8511	5.2198	11.2573	0.20	0.54	1.00	2.8512	11.0948	0.30	0.26	0.90

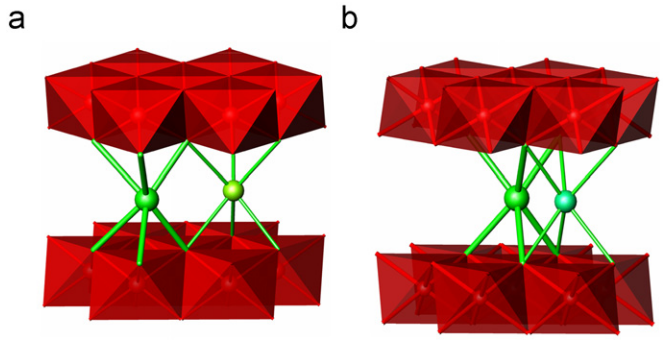

Fig. 2. Schematic representation of two sodium positions in orthorhombic (a) and hexagonal (b) modifications of $Na_{2/3}MnO_2$. Red and green colours correspond to Mn and Na, respectively. (For interpretation of the references to colour in this figure legend, the reader is referred to the web version of this article.)

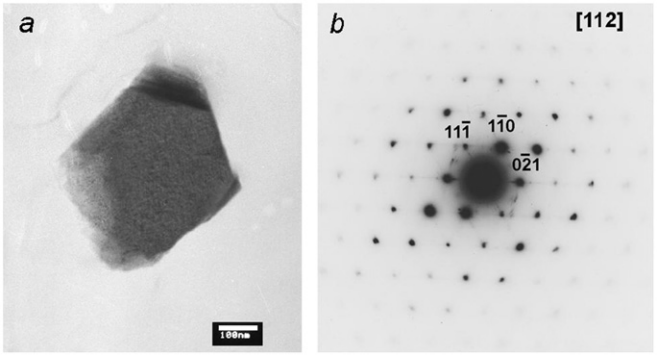

Fig. 3. Bright field micrograph of *NMO-1000* (a). Selected area electron diffraction (SAED) of *NMO-1000* particle along [112] orientation in the orthorhombic structure (*Cmcm* space group, b).

repulsions and in-plane Na^+–Na^+ (Li^+–Li^+) electrostatic repulsions [29]. Based on first-principles investigations of phase stability in the *O*2–$LiCoO_2$ system, it has been shown for the first time that the reduction of the in-plane Li^+–Li^+ electrostatic repulsions can be achieved by simultaneous occupancies of both sites instead of energetically most favorable site [28]. By single crystal neutron diffraction [30], it has been demonstrated that the occupancy of the *Na*(1) site is promoted by the creation of multi-vacancy clusters in *Na*(2) sites.

In addition, low intensive peaks at 23.9°, 33.2° and 42.6° are also observed. These peaks can be related tentatively with an impurity phase such as bixbyite Mn_2O_3 (ref. code 00-002-0909). However, the appearance of a superstructure (with a space group different from *Cmcm*) cannot be rejected. In order to understand this result, electron diffraction was undertaken (Fig. 3). The bright field image demonstrates that *NMO-1000* consists of well-shaped hexagonal particles with mean dimensions of about 500 nm. Fig. 3 shows the selected area electron diffraction (SAED) pattern of the *NMO-1000* particle taken along the [1 1 2] zone axis direction. All diffraction spots are indexed using an orthorhombic unit cell with parameters identical with that determined from powder XRD experiments. This means that low intensive peaks are due to an impurity phase rather than a superstructure.

For samples annealed at lower temperatures, a new phase grows in intensity (Fig. 1). The crystal structure of the second phase is refined in the $P6_3/mmc$ space group. The hexagonal structure has already been reported for Na_xMnO_2 with $x<0.7$ [14]. The amount of the hexagonal modification is higher for the sample annealed at 420 °C (Table 1). In the same sequence, the oxidation state of Mn smoothly increases (Table 1). It is noticeable that, under these conditions, there is a mixture

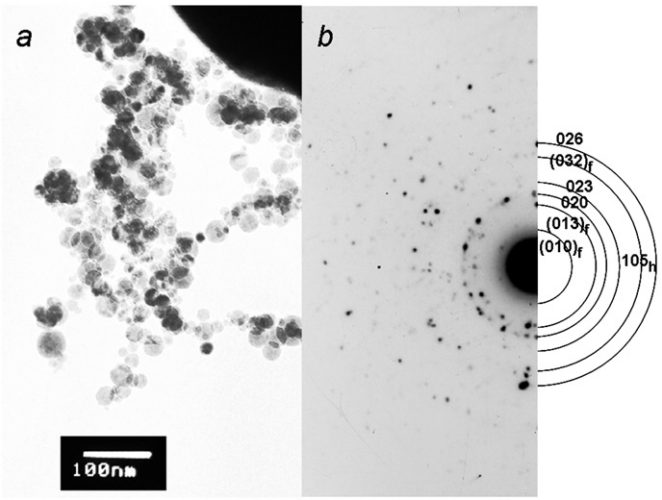

Fig. 4. Bright field micrograph of *NMO-420* (a). Polycrystalline electron diffraction (b) corresponding to the mixture of orthorhombic (allowed and forbidden reflections) and the hexagonal (105_h) phases.

between orthorhombic and hexagonal forms. Fig. 4 gives the bright field image of *NMO-420*. The oxide annealed at 420 °C consists of spherical particles with dimensions lower than 100 nm. The polycrystalline electron diffraction reveals that *NMO-420* is a mixture between orthorhombic and hexagonal phases, which is consistent with the powder XRD data.

For the hexagonal modification, the refinement result is improved when the site occupancy of Mn is less than one: $R_b=7.90$ and $R_f=5.37$ becomes $R_b=6.40$ and $R_f=4.72$ when the Mn occupancy is refined (Table 1). For the orthorhombic modification, the refinement of the Mn occupancy shows that the occupancy remains close to 1. Further slight improvement of the refinement result for the hexagonal phase is gained when the *Na*(2) site is displaced from the centre of the ideal triangular prismatic *2d* site at (2/3, 1/3, 0.25) to 6 h site at (2*z*, *z*, 0.25). When $z=1/3$, then the 6 h site converges within 2*d* site. Fixing the Mn and Na occupancies in hexagonal Na_xMnO_2, the refined *z*-value tends to 0.31(2). The same feature has been established for structurally related Na_xCoO_2 with $0.34\le x\le 0.75$, where *z* varies between 0.27 and 0.29 [31]. It is worth mentioning that sodium occupancy in the first position (energetically unfavourable) is higher in comparison with that in the second position. The displacement of *Na*(2) from the triangular prismatic site as well as the deviation of the Mn occupancy from 1 suggest some structural peculiarities in the hexagonal Na_xMnO_2 modification, which will be discussed in the next section.

Structural parameters of annealed samples are compared in Table 1. It appears that below 700 °C the unit-cell volume of the orthorhombic phase increases, whereas the hexagonal modification displays a lattice contraction (Table 1). Taking into account the higher overall oxidation state of Mn (Table 1), the observed changes in the unit cell volumes suggest that the orthorhombic and hexagonal phases exhibit different amounts of Mn^{4+} ions. Due to the smaller ionic radius of Mn^{4+}, the unit-cell volume contraction indicates a higher Mn^{4+} content in the hexagonal Na_xMnO_2 in comparison with that of the orthorhombic phase. This means that Mn^{4+} ions are preferentially stabilized in the hexagonal modification.

To rationalize the temperature-induced phase transformation, Raman scattering experiment was undertaken. Fig. 5 compares the Raman spectra of *NMO-1000* and *NMO-420*. The Raman spectrum of *NMO-1000* consists of two intense bands at 580 and 327 cm^{-1} together with two weaker bands at 630 and 431 cm^{-1}

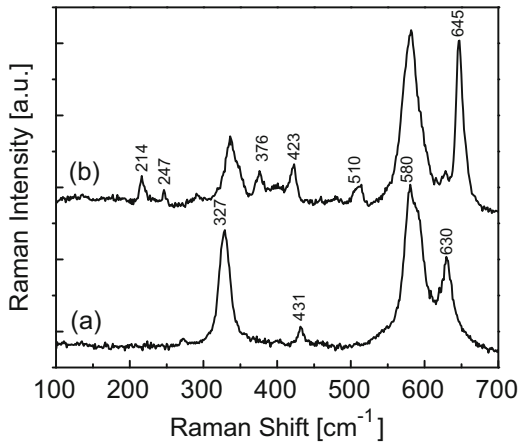

Fig. 5. Raman spectra of *NMO-1000* (a) and *NMO-420* (b).

and a shoulder at about 590 cm^{-1}. When $Na_{2/3}MnO_2$ is annealed at 420 °C, the Raman spectrum undergoes significant changes. In addition to the bands of *NMO-1000*, new bands at 645, 510, 423, 376 and 247/214 cm^{-1} are clearly resolved. For *NMO-420*, high-frequency peak at 645 cm^{-1} displays a strong intensity. It is worth mentioning that the Raman bands of both *NMO-1000* and *NMO-420* samples are not perturbed by the bixbyite impurity. In the literature, different Raman spectra (in respect of peak positions) of Mn_2O_3 are reported [32–36]: bands at 565, 620 and 672 cm^{-1} [32]; bands at 192, 314, 481, 592, 645 and 698 cm^{-1} [33], and bands at 307, 341, 637 and 688 cm^{-1} [34–36]. In addition, bixbyite is black, as a result of which the Raman scattering is very weak [32]. Since the Raman spectra of *NMO-1000* and *NMO-420* do not display any peaks at a frequency higher than 640 cm^{-1}, it seems that the bixbyite impurity does not affect the Raman bands of $Na_{2/3}MnO_2$.

Detailed Raman spectroscopy studies on sodium cobaltate analogues, Na_xCoO_2, serve as a basis to assign the Raman modes observed for $Na_{2/3}MnO_2$ samples [37–44]. Three structural modifications have been established for Na_xCoO_2 ($x<1$): hexagonal, orthorhombic and monoclinic phases. For hexagonal Na_xCoO_2 with $P6_3/mmc$ space group, factor group analysis predicts five Raman active modes: an A_{1g} and an E_{1g} mode due to O vibrations and three E_{2g} modes due to Na and O vibrations. The Co vibrations are not Raman active. The A_{1g} and E_{1g} modes are unambiguously detected in the Raman spectra of Na_xCoO_2, while there are contradictions concerning the assignment of the three E_{2g} modes. This fact has been explained by the mobility of Na among the different lattice sites [42]: the three E_{2g} modes can be observed in the case when Na^+ ions have a lower mobility and are distributed in an ordered way. The strongest peak is due to the A_{1g} mode and appears at high frequency. In contrast to Na_xCoO_2, in our experiment hexagonal Na_xMnO_2 presents the five Raman modes if we assign all the new bands in the spectrum of *NMO-420* to it. The strongest peak at high frequency is the 645 cm^{-1} one. This allows assigning the band to the A_{1g} mode. The appearance of five Raman bands points at the more ordered distribution of Na^+ in interlayers of $Na_{2/3}MnO_2$ in comparison with the Co analogues.

Contrary to hexagonal Na_xCoO_2, there are few papers in the literature concerning the Raman characterization of orthorhombic Na_xCoO_2. From factor group analysis, an increase of the number of Raman active phonon modes is expected. However, for orthorhombic Na_xCoO_2 with *Cmcm* space group, two intensive bands at 570 and 450 cm^{-1} have been detected by Zhou et al. [15]. The orthorhombic Na_xCoO_2 phase with *Pmmm* space group displays only three intense bands at 570, 476 and 439 cm^{-1} [39]. In comparison with Na_xCoO_2, the observed bands at 630, 580, 431 and 327 cm^{-1} in the spectrum of *NMO-1000* can be attributed to orthorhombic Na_xMnO_2, which is a single phase according to the XRD analysis. However, for the orthorhombic modification (*Cmcm* space group), nine Raman active modes are expected to be active: $3A_g+2B_{1g}+B_{2g}+3B_{3g}$. The different number of observed and predicted Raman modes does not allow assigning them exactly.

For the monoclinic modification of $Na_{0.6}CoO_2$ (*C2/m* space group), nine Raman active modes are suggested: $5A_g+4B_g$. However, only three bands have been observed: 691, 577 and 461 cm^{-1} [41]. Above 350 K, the monoclinic phase is reversibly converted into a rhombohedral phase (*R*-3 m space group) [29]. The rhombohedral phase displays two Raman modes at 586 and 486 cm^{-1}, as was predicted by the factor group analysis [41]. It is worth mentioning that monoclinic distortion in Co phases is stronger than that of Mn-phases: $\beta=106.069$ and $\beta=90.68°$, respectively [29,12]. Therefore, the observation of four well defined Raman modes in *NMO-1000* can be related with orthorhombic phase instead of monoclinic phase. Furthermore, the refinement of Na_xMnO_2 with a monoclinic structure does not give satisfactory results.

3.2. Structural characterization of $Na_{2/3}MnO_2$ by EPR

Fig. 6 compares the EPR spectra of *NMO-1000*, *NMO-700* and *NMO-420*. In the temperature range 300–70 K, the EPR spectrum of the orthorhombic modification *NMO-1000* consists of a broad Lorentzian line with an effective *g*-factor of 1.72 and a line with $\Delta H_{pp}\approx 300$ mT. Below 70 K, the signal is broadened and disappears at $T<50$ K. The temperature behavior of the EPR signal is consistent with a temperature dependence of the magnetic susceptibility

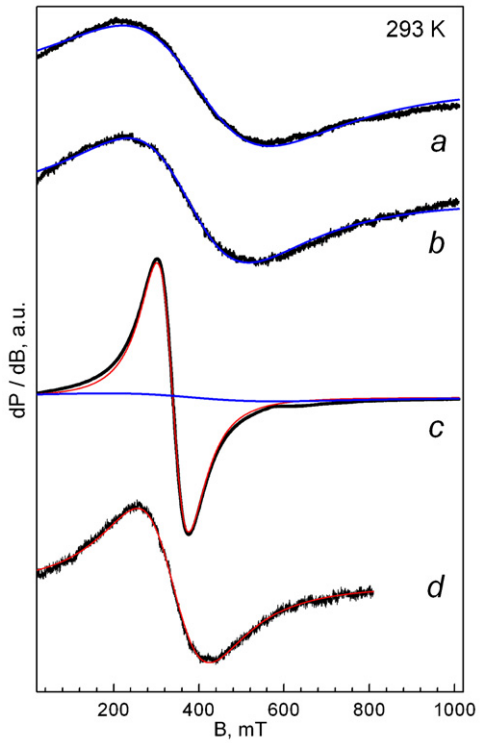

Fig. 6. EPR spectra of $Na_{2/3}MnO_2$ quenched from 1000 °C (a), 700 (b) and 420 °C (c) and of $Na_{2/3}Co_{2/3}Mn_{1/3}O_2$ standard (d). The blue and red lines correspond to the simulated Lorentzian signal due to the orthorhombic and hexagonal modifications, respectively. (For interpretation of the references to colour in this figure legend, the reader is referred to the web version of this article.)

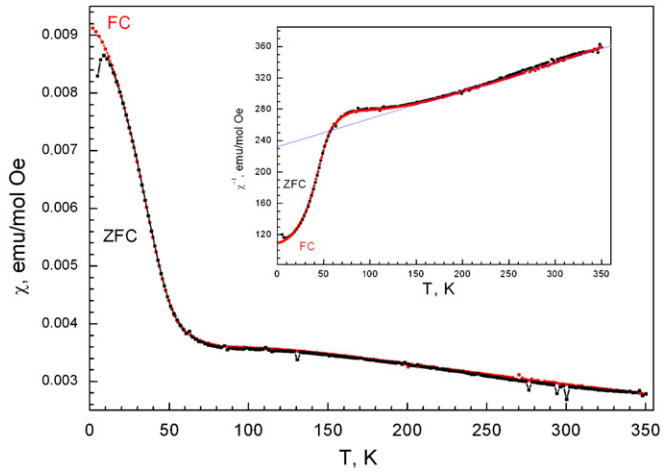

Fig. 7. Temperature dependence of the zero-field cooled (ZFC) and field-cooled (FC) magnetic susceptibility of $Na_{2/3}MnO_2$ quenched from 1000 °C in an applied magnetic field of 500 mT. The inset shows the inverse susceptibilities with a Curie–Weiss law above 160 K.

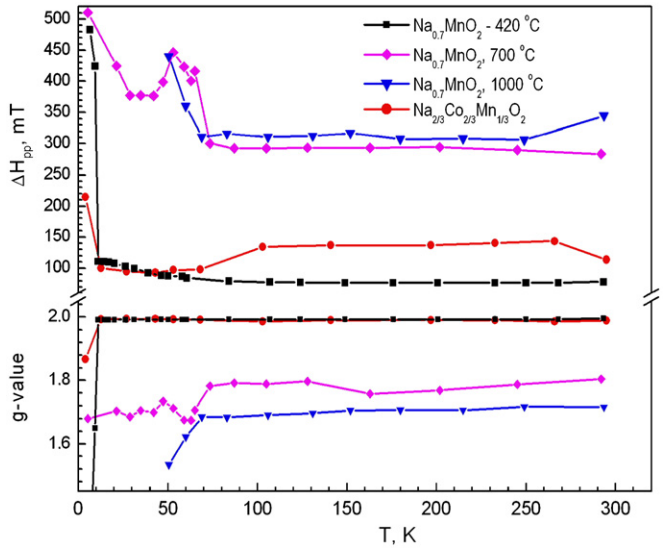

Fig. 8. Temperature dependence of the EPR line width, ΔH_{pp}, and the *g*-factor of $Na_{2/3}MnO_2$ quenched from 1000 °C, 700 and 420 °C and hexagonal $Na_{2/3}Co_{2/3}Mn_{1/3}O_2$.

(Fig. 7). In the limited temperature range 350–160 K, the Curie–Weiss law (with Curie and Weiss constants of 0.38 and −648 K, respectively) is obeyed. The large Weiss constant reveals a development of strong antiferromagnetic interactions between manganese ions in $Na_{2/3}MnO_2$. The magnetic susceptibility displays slight temperature dependence between 130 and 70 K, while below 70 K there is a strong increase of the magnetic susceptibility. A divergence between ZFC and FC susceptibilities is observed below 9 K, where the ZFC susceptibility reaches a maximum value on application of a magnetic field of 500 mT. The observed temperature behavior indicates a spin-glass transition at 9 K. The magnetic susceptibility data allow associating the broad EPR signal observed between 300 and 70 K to the total magnetic moment of the Mn^{3+}–Mn^{4+} spin system.

For *NMO-700*, the broad signal is still observed. Since this sample is a two phase mixture (Fig. 1), the observation of one signal can be understood if we take into account the temperature variation of the resonance absorption and of the EPR line width (Fig. 8). The abrupt changes in line width and effective *g*-factor at about 50 K coincide with those observed for the pure orthorhombic modification. Contrary to *NMO-1000*, the broad signal of *NMO-700* does not disappear below 50 K. Therefore, the observed signal between 50 and 10 K can be related with the hexagonal modification. However, the accurate determination of the EPR parameters of the hexagonal modification is obscured due to the presence of an orthorhombic modification characterized with increased magnetic susceptibility.

The EPR spectrum undergoes strong changes when $Na_{2/3}MnO_2$ is annealed at 420 °C. Two overlapping Lorentzian signals characterized by different *g*-values and line widths are distinguished (Fig. 6). The first signal is broader and possesses an EPR line width and an effective *g*-factor comparable with that due to the Mn^{3+}–Mn^{4+} spin system: $g \approx 1.77(2)$ and $\Delta H_{pp} \approx 395(4)$ mT (Fig. 8). The second signal displays a *g*-value of 1.996(1) and a line width of 75(1) mT that remain nearly constant in the temperature range 12–300 K (Fig. 8). These parameters are typical of Mn^{4+}. To rationalize the EPR spectrum of *NMO-420*, we used $Na_{2/3}Mn_{1/3}Co_{2/3}O_2$ as EPR standard for Mn^{4+} surrounded by diamagnetic Co^{3+} and identical paramagnetic Mn^{4+} ions. The appearance of diamagnetic Co^{3+} and paramagnetic Mn^{4+} is proven by the temperature dependence of the magnetic susceptibility. In the temperature range 300–50 K, the magnetic susceptibility obeys the Curie–Weiss law with a Curie constant of 0.563 and a Weiss constant of −25.5 K, respectively. The Curie constant determined from the magnetic susceptibility measurement is close to the theoretical one calculated assuming the appearance of diamagnetic Co^{3+} and paramagnetic Mn^{4+} ions: 0.625. The EPR spectrum of $Na_{2/3}Mn_{1/3}Co_{2/3}O_2$ shows one narrow Lorentzian line due to Mn^{4+} ions. The temperature dependences of the EPR line width and the *g*-factor are shown in Fig. 8. As one can see, the EPR parameters of two signals detected with $Na_{2/3}Mn_{1/3}Co_{2/3}O_2$ and hexagonal Na_xMnO_2 are alike. This means that Mn^{4+} ions only give rise to the EPR profiles. In addition, the *g*-value of Mn^{4+} in $Na_{2/3}Mn_{1/3}Co_{2/3}O_2$ is slightly lower as compared to that of hexagonal Na_xMnO_2: 1.991(1) and 1.996(1), respectively. The different *g*-values of Mn^{4+} reflect the nature of the Mn–O bonding in the two layered phases. For hexagonal Na_xMnO_2, the deviation of the *g*-value from the *g*-factor of the free electron ($g=2.0023$) is lower, indicating an increased covalency of the Mn–O bond. For $Na_{2/3}Mn_{1/3}Co_{2/3}O_2$, the stronger deviation of the *g*-value of Mn^{4+} from 2.0023 indicates a less covalent Mn–O bond character. In addition, this is consistent with the different Mn–O bond lengths established for the two phases: the Mn–O bond length is 1.91 Å for $Na_{2/3}Mn_{1/3}Co_{2/3}O_2$ [24] and 1.87 Å for hexagonal $Na_{2/3}MnO_2$. For the sake of comparison, the *g*-value of Mn^{4+} in other layered oxides based on cobalt and manganese are as follows: the isotropic *g*-value is 1.983 for Mn^{4+} in CoO_2-layers ($LiCoO_2$, [45]) and $g=1.996$ for Mn^{4+} in $Li_{1/3}Mn_{2/3}O_2$-layers (monoclinic Li_2MnO_3, [46,47]). Taking into account the *g*-values of Mn^{4+} in $LiCoO_2$, $Na_{2/3}Mn_{1/3}Co_{2/3}O_2$, hexagonal Na_xMnO_2 and Li_2MnO_3 matrices, it appears that there is a clear tendency for increasing the *g*-value of Mn^{4+} ions when going from pure Co to pure Mn nearest environment. This means that the Mn–O bond becomes more covalent in the case when Mn^{4+} is surrounded by identical manganese ions.

From the comparative EPR analysis, it appears that the hexagonal modification only contains Mn^{4+} ions, which are not surrounded by Mn^{3+} ions. In this case, the compensation of Mn^{4+} charge can be achieved either by extraction of Na^+ from Na-layers or by creation of Mn-vacancies. The exsolution of Na from Na-layers as a separate Na_2CO_3 phase has recently been established for the sodium cobaltate Na_xCoO_2 during its slow cooling from 800 °C [15]. For Na_xMnO_2, there is not any contamination due to Na_2CO_3. This is demonstrated by the lack of the characteristic infra-red mode ($\approx 860\,cm^{-1}$) of the carbonate ions in the IR

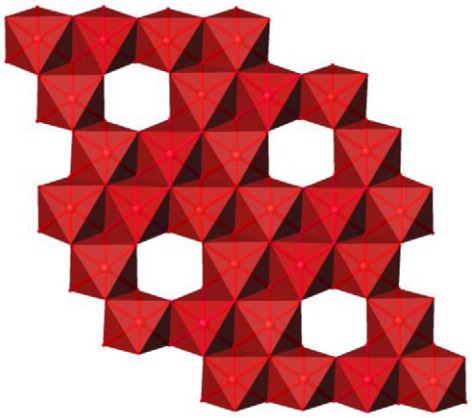

Fig. 9. Schematic view of the vacancy distribution in the manganese layer of $Na_2Mn_3O_7$ [50]. MnO_6 octahedral are denoted with red colour. (For interpretation of the references to colour in this figure legend, the reader is referred to the web version of this article.)

spectrum of Na_xMnO_2 (not shown). Keeping the Na-to-Mn ratio, the charge compensation could be achieved by creation of vacancies in the manganese layer. In the framework of layered structure, the structural formula of *NMO-420* can be presented by $Na^+_{4x}[Mn^{4+}_{1-x}\square_x]O_2$ with vacancies in the transition metal layer. Taking into account the site occupancy determined from Rietveld analysis (Table 1), it is possible to evaluate the composition of $Na_{0.7}MnO_2$ annealed at 420 °C: $Na_{0.58}[Mn_{0.86}\square_{0.14}]O_2$. The similar EPR parameters of the isostructural $Na^+_{4x}[Mn^{4+}_{1-x}\square_x]O_2$ and $Na_{2/3}Mn_{1/3}Co_{2/3}O_2$ imply that the manganese vacancies are disordered in the hexagonal modification of $Na^+_{4x}[Mn^{4+}_{1-x}\square_x]O_2$. Furthermore, the appearance of vacancies in the Mn-layers will force the occupancy of *Na*(1) position sharing faces with manganese octahedra (Fig. 2). This is consistent with the interlayer distribution of Na in *NMO-420*, where the energetically unfavourable *Na*(1) site is heavily occupied (Table 1).

The appearance of vacancies in the Mn-layers is not a unique feature of $Na_{2/3}MnO_2$. The formation of manganese deficient layers has been reported for sodium manganese oxides $Na_2Mn_3O_7$ obtained under high pressure (1.4 kbar) [48–50]. The structure is composed of infinite Mn_3O_7-sheets, where only 6/7 of the sites are occupied by Mn^{4+} ions in a regular manner. Similar to the case of a hexagonal type structure, the structure of $Na_2Mn_3O_7$ can also be presented as $Na_{4/7}[Mn_{6/7}\square_{1/7}]O_2$ built by MnO_2 layers of edge-sharing MnO_6 octahedra, in which every seventh Mn^{4+} ion is removed from the layer in such a way as to create an ordered distribution of vacancies (Fig. 9, [50]). These values of manganese vacancies are comparable to that determined by us for the low-temperature hexagonal modification of $Na^+_{4x}[Mn^{4+}_{1-x}\square_x]O_2$: $x \approx 0.14$. The difference in the cationic distribution between $Na_2Mn_3O_7$ and $Na^+_{4x}[Mn^{4+}_{1-x}\square_x]O_2$ is a consequence of the manner of vacancies arrangement. A structure consisting of vacant Mn-layers has also been established for sodium birnessite and chalcophanite, $ZnMn_3O_7(H_2O)_3$ [51,52]. The octahedral layers of $ZnMn_3O_7(H_2O)_3$ have vacancies in one-seventh of the Mn sites, with interlayer zinc cations residing above and below these vacancies [52]. Sodium birnessite displays a similar layered structure characterized with a small fraction of Mn vacancies and only one interlayer plane containing both the cations and the water molecules [51,53]. It is assumed that Mn vacancies in an amount of about 10–15% are randomly distributed over the layers [51,53]. In addition, it is worth mentioning that the crystal structure of synthetic and natural birnessites is still under debate [51,53,54]. Using HRTEM lattice images, it has been suggested that there are no vacancies in the octahedral layers of synthetic birnessite [54]. However, it is hard to distinguish whether the vacancies in the Mn-layers are defects or characteristic structural features of birnessite [54].

Returning to the samples studied by us, the EPR analysis shows that the hexagonal modification annealed at 700 °C displays quite different EPR parameters in comparison with the hexagonal modification annealed at 420 °C. This clearly indicates a different Mn environment (in terms of Mn^{4+} and Mn^{3+} neighbours) in both types of oxides. The simultaneous appearance of Mn^{4+} and Mn^{3+} ions in hexagonal oxides annealed at 700 °C leads to a deviation of the *g*-value from that of Mn^{4+}, as well as to an increase in the EPR line width (Fig. 8).

3.3. Stabilization of over-stoichiometric Mn^{4+} in $Na_{2/3}MnO_2$

Based on the structural and EPR results, it is now possible to discuss the stabilization of over-stoichiometric Mn^{4+} in $Na_{2/3}MnO_2$ compositions. The orthorhombic modification with a nominal composition $Na_{2/3}MnO_2$ is formed at 1000 °C, where Mn^{4+} ions, in addition to Mn^{3+}, compensate for the sodium deficiency: $Na_{2/3}[Mn^{3+}_{2/3}Mn^{4+}_{1/3}]O_2$. With lowering quenching temperature, a phase separation into an orthorhombic and a hexagonal modification takes place, concomitant with an increase in the oxidation state of Mn over the stoichiometric one. The over-stoichiometric highly oxidised Mn ions are preferentially accommodated by the hexagonal modification. The charge compensation proceeds by creation of vacancies in the manganese layers, culminating at 420 °C in the formation of layers only containing Mn^{4+} ions and vacancies. In the framework of the layered structure, the over-stoichiometric Mn^{4+} ions which are needed to compensate the excess of oxygen uptake during slow cooling can be expressed as follows: $Na_{2/3(1-x)}[Mn^{3+}_{2/3-5x}Mn^{4+}_{1/3+4x}\square_x]O_2$, where $x=2/15$ for the oxides annealed at 420 °C and for the oxides quenched from 1000 °C $x \to 0$.

The effect of the cooling rate on the structure and composition has also been reported for sodium cobaltates, Na_xCoO_2 with $x \sim 0.65$ [15]. When Na_xCoO_2 is slowly cooled from 800 °C, an exsolution of Na takes place and a separate sodium carbonate phase, Na_2CO_3, appears. As a result, the slowly cooled Na_xCoO_2 sample adopts a hexagonal structure ($P6_3/mmc$) with a lower Na content ($x \sim 0.63$), whereas the quenched sample exhibits an orthorhombic distorted structure (*Cmcm*) with higher Na content ($x \sim 0.68$). In comparison with Na_xCoO_2, slow cooling of Na_xMnO_2 leads to the allocation of Mn^{4+} among orthorhombic and hexagonal structure with keeping the Na-to-Mn ratio.

4. Conclusion

The crystal structure and composition of $Na_{2/3}MnO_2$ display a strong dependence on the history of the thermal treatment. The orthorhombic distorted modification is stabilized at high temperatures (1000 °C). At lower quenching temperature, there is a phase separation into an orthorhombic and a hexagonal modification, concomitant with an increase in the oxidation state of Mn. The hexagonal modification is able to accommodate the over-stoichiometric Mn^{4+} ions by creation of vacancies in the MnO_2-layers. The appearance of vacancies in the Mn-layers forces the occupancy of the *Na*(1) position that shares common faces with the manganese octahedra.

Acknowledgments

This work was supported by the National Science Fund of Bulgaria: project IDEAS No D002-309/2008. The Raman

equipment is used in the framework of project Integrated Research Centres at the Universities No DO02-167/2008. R.S. is grateful to CNRS for a research stay in ICMCB, Bordeaux, France. Dr. M. Ménétrier and Dr. L. Croguennec (ICMCB-CNRS) are deeply acknowledged for fruitful discussions. The authors also thank Cathy Denage (ICMCB-CNRS) for the sample preparation. R.S., E.Zh. and M.Y. are grateful to the National Centre for New Materials (DO-02-82/2008).

Appendix A. Supplementary materials

Supplementary data associated with this article can be found in the online version at doi:10.1016/j.jssc.2010.04.024

References

[1] J.-P. Parant, R. Olazcuaga, M. Devalette, C. Fouassier, P. Hagenmuller, J. Solid State Chem. 3 (1971) 1.
[2] C. Fouassier, C. Delmas, P. Hagenmuller, Mater. Res. Bull. 10 (1975) 443.
[3] A. Robert Armstrong, P.G. Bruce, Nature 381 (1996) 499.
[4] M.S. Whittingham, P.Y. Zavalij, Solid State Ionics 131 (2000) 109–115.
[5] I. Terasaki, Y. Sasago, K. Uchinokura, Phys. Rev. B 56 (1997) R12685.
[6] Y. Wang, N.S. Rgado, R.J. Cava, N.P. Ong, Nature 423 (2003) 425.
[7] K. Takada, H. Sakurai, E. Takayama-Muromachi, F. Izumi, R.A. Dilanian, T. Sasaki, Nature 422 (2003) 53.
[8] L.B. Luo, Y.G. Zhao, G.M. Zhang, S.M. Guo, Z. Li, J.L. Luo, Phys. Rev. B 75 (2007) 125115.
[9] A. Mendiboure, C. Delmas, P. Hagenmuller, J. Solid State Chem. 57 (1985) 323.
[10] C. Delmas, C. Fouassier, P. Hagenmuller, Physica B+C 91 (1980) 81.
[11] L. Bordet-Le Guenne, P. Deniard, P. Biensan, C. Siret, R. Brec, J. Mater. Chem. 10 (2000) 2201.
[12] J.M. Paulsen, J.R. Dahn, Solid State Ionics 126 (1999) 3.
[13] Y.U. Jeong, A. Manthiram, J. Solid State Chem. 156 (2001) 331.
[14] A. Caballero, L. Hernán, J. Morales, L. Sánchez, J. Santos Peña, M.A.G. Aranda, J. Mater. Chem. 12 (2002) 1142.
[15] T. Zhou, D. Zhang, T.W. Button, A.J. Wright, Colin Greaves, J. Mater. Chem. 19 (2009) 1123.
[16] D. Pasero, N. Reeves, L.J. Gillie, A.R. West, J. Power Sources 174 (2007) 1078.
[17] J. Krzystek, J.-H. Park, M.W. Meisel, M.A. Hitchman, H. Stratemeier, L.-C. Brunel, J. Tesler, Inorg. Chem. 41 (2002) 4478.
[18] R. Stoyanova, M. Gorova, E. Zhecheva, J. Phys. Chem. Solids 61 (2000) 609.
[19] D. Capsoni, M. Bini, G. Chiodelli, V. Massarotti, M.C. Mozatti, A. Comin, Phys. Chem. Chem. Phys. 3 (2001) 2162.
[20] D. Capsoni, M. Bini, G. Chiodelli, V. Massarotti, M.C. Mozatti, C. Azzoni, Solid State Commun. 125 (2003) 179.
[21] E. Zhecheva, R. Stoyanova, Solid State Commun. 135 (2005) 405.
[22] E. Zhecheva, M. Gorova, R. Stoyanova, J. Mater. Chem. 9 (1999) 1559.
[23] E. Zhecheva, R. Stoyanova, M. Gorova, P. Lavela, J.-L. Tirado, Solid State Ionics 140 (2001) 19.
[24] F. Tournadre, L. Croguennec, I. Saadoune, F. Weill, Y. Shao-Horn, P. Willmann, C. Delmas, Chem. Mater. 16 (2004) 1411.
[25] L.D. Dyer, B.S. Borie, G.P. Smith, J. Am. Chem. Soc. 76 (1954) 1499.
[26] O. Haas, Chr. Ludwig, A. Wokaun, Anal. Chem. 78 (2006) 7273.
[27] J. Rodríguez-Carvajal, Satellite Meeting on Powder Diffraction of the XV Congress of the IUCr, 1990, p. 127.
[28] D. Carlier, A. Van der Ven, C. Delmas, G. Ceder, Chem. Mater. 15 (2003) 2651.
[29] M. Blangero, D. Carlier, M. Pollet, J. Darriet, C. Delmas, J.-P. Doumerc, Phys. Rev. B 77 (2008) 184116.
[30] M. Roger, D.J.P. Morris, D.A. Tennant, M.J. Gutmann, J.P. Goff, J.-U. Hoffmann, R. Feyerherm, E. Dudzik, D. Prabhakaran, A.T. Boothroyd, N. Shannon, B. Lake, P.P. Deen, Nature 445 (2007) 631.
[31] Q. Huang, M.L. Foo, R.A. Pascal Jr., J.W. Lynn, B.H. Toby, Tao He, H.W. Zandbergen, R.J. Cava, Phys. Rev. B 70 (2004) 184110.
[32] W.B. White, V.G. Keramidas, Spectrochim. Acta A 28 (1972) 501.
[33] C.M. Julien, M. Massot, C. Poinsignon, Spectrochim. Acta A 60 (2004) 689.
[34] Y.T. Chua, P.C. Stair, I.E. Wachs, J. Phys. Chem. B 105 (2001) 8600.
[35] F. Buciuman, F. Patcas, R. Cracium, D.R.T. Zahn, Phys. Chem. Chem. Phys. 1 (1999) 185.
[36] Y.-F. Han, L. Chen, K. Ramesh, Z. Zhong, F. Chen, J. Chin, H. Mook, Catal. Today 131 (2008) 35.
[37] M.N. Iliev, A.P. Litvinchuk, R.L. Meng, Y.Y. Sun, J. Cmaidalka, C.W. Chu, Physica C 402 (2004) 239.
[38] Y.G. Shi, Y.L. Liu, H.X. Yang, C.J. Nie, R. Jin, J.Q. Li, Phys. Rev. B 70 (2004) 052502.
[39] H.X. Yang, C.J. Nie, Y.G. Shi, H.C. Yu, S. Ding, Y.L. Liu, D. Wu, N.L. Wang, J.Q. Li, Solid State Commun. 134 (2005) 403.
[40] X.N. Zhang, P. Lemmens, V. Gnezdilov, K.Y. Choi, B. Keimer, D.P. Chen, C.T. Lin, F.C. Chou, Physica B 359-361 (2005) 424.
[41] H.X. Yang, Y. Xia, Y.G. Shi, H.F. Tian, R.J. Xiao, X. Liu, Y.L. Liu, J.Q. Li, Phys. Rev. B 74 (2006) 094301.
[42] J.F. Qu, W. Wang, Y. Chen, G. Li, X.G. Li1, Phys. Rev. B 73 (2006) 092518.
[43] F.X. Zhang, S.K. Saxena, C.S. Zha, J. Solid State Chem. 180 (2007) 1759.
[44] T. Wu, K. Liu, H. Chen, G. Wu, Q.L. Luo, J.J. Ying, X.H. Chen, Phys. Rev. B 78 (2008) 115122.
[45] R. Stoyanova, A.-L. Barra, M. Yoncheva, E. Zhecheva, E. Shinova, P. Tzvetkova, S. Simova, Inorg. Chem. 49 (2010) 1932.
[46] V. Massarotti, D. Capsoni, M. Bini, C.B. Azzoni, J. Solid State Chem. 128 (1997) 80.
[47] R. Stoyanova, E. Zhecheva, M. Gorova, J. Mater. Chem. 10 (2000) 1377.
[48] A.P. Ramirez, Annu. Rev. Mater. Sci. 24 (1994) 453.
[49] F.M. Chang, M. Jansen, Z. Anorg. Allg. Chem. 531 (1985) 177.
[50] E.A. Raekelboom, A.L. Hector, J. Owen, G. Vitins, M.T. Weller, Chem. Mater. 13 (2001) 4618.
[51] E.J. Silvester, A. Manceau, V.A. Drits, Am. Mineral. 82 (1997) 962.
[52] S. Ching, D.J. Petrovay, M.L. Jorgensen, S.L. Suib, Inorg. Chem. 36 (1997) 883.
[53] B. Lanson, V.A. Drits, A.-C. Gaillot, E. Silvester, A. Plançon, A. Manceau, Am. Mineral. 87 (2002) 1631.
[54] D.S. Yang, M.K. Wang, Chem. Mater. 13 (2001) 2589.